March 17, 2000

Thermal chain model of electro- and magnetorheology

James E. Martin

Sandia National Laboratories

Albuquerque, New Mexico 87185-1421

Abstract: Steady shear 3-D simulations of electro- and magnetorheology in a uniaxial field are presented. These large scale simulations are three dimensional, and include the effect of Brownian motion. In the absence of thermal fluctuations, the expected shear thinning viscosity is observed in steady shear, and a striped phase is seen to rapidly form in a uniaxial field, with a shear slip zone in each sheet. However, as the influence of Brownian motion increases, the fluid stress decreases, especially at lower Mason numbers, and the striped phase eventually disappears, even when the fluid stress is still high. To account for the uniaxial steady shear data we propose a microscopic chain model of the role played by thermal fluctuations on the rheology of ER and MR fluids that delineates the regimes where an applied field can impact the fluid viscosity, and gives an analytical prediction for the thermal effect.

DISCLAIMER

DISCLAIMER

Portions of this document may be illegible in electronic image products. Images are produced from the best available original document.

I. INTRODUCTION

The rheology of electrorheological (ER) and magnetorheological (MR) suspensions is characterized by a shear thinning viscosity, but the mechanism by which this occurs is still at issue, especially when thermal fluctuations play a significant role. To investigate this, we have conducted 3-D Brownian dynamics simulations of the field-induced rheology of suspensions subjected to uniaxial fields. When thermal fluctuations are small the formation of a striped phase is observed, in which sheets form orthogonal to the axis of fluid vorticity of the shearing fluid. But as thermal fluctuations increase in a uniaxial field, the striped phase disappears well before the fluid stress does, and the stress is reduced most greatly at the lowest shear rate. A thermal chain model is developed to describe these data, which is an extension of the athermal chain model [1].

There have been a number of interesting simulation studies of field-induced rheology in a uniaxial field. Whittle [2] developed a 3-D Brownian dynamics simulation method with N=216 particles in steady shear and found the formation of a striped phase, which was thought possibly an artifact of the cyclic boundary conditions in these small scale simulations. Melrose [3] conducted free draining (no hydrodynamic interactions) 3-D Brownian dynamics simulations in steady shear with 108 particles at 31 vol.%, and determined a phase diagram in λ, Pe space, where λ is the dimensionless ratio of the dipolar interaction energy to the thermal energy, and Pe is the Peclet number, the ratio of the hydrodynamic forces to the thermal forces. Melrose found that when the Mason number - the ratio of the hydrodynamic to dipolar forces - exceeded the critical Mason number, above which particles cannot chain, a sheared string phase formed. At lower Mn and for large λ, a layered flowing crystalline phase formed, which is also known as a striped phase. At low values of λ, and low Pe, only a disordered liquid phase was found. Stress computations showed a shear thinning viscosity. This work was later extended [4] to larger system sizes (N=256), with similar conclusions, and finally to particle volume fractions of 10% and 50%, still larger systems (N=500), and hard sphere interactions [5].

Melrose found that the smaller-than-expected shear thinning exponents sometimes observed in experiments at low λ [6] were due to thermal fluctuations. At the volume fraction of 50% a layered phase was not found. The work of Melrose was continued by Guo et al. [7] who obtained consistent results.

Bonnecaze and Brady [8] conducted 2-D athermal "Stokesian" dynamics simulations, with a highly accurate treatment of the hydrodynamic and electrostatic interactions. System sizes were consequently small - 25 particles - and of course, a striped phase could not form, but they did find the expected shear thinning viscosity. Thermal fluctuations were later added, [9] and shear thinning exponents smaller than 1.0 were observed, in agreement with the results of Melrose. A phenomenological description of the thermal effect was argued, in a physical picture where shear flow is caused by particles hopping out of potential wells.

Work on oscillatory shear appears to be restricted to Parthasarathy and Klingenberg, who, in addition to work in steady shear [10], conducted 2-D athermal dynamics simulations in oscillatory shear with N=250 particles [11]. Simulations with and without hydrodynamics interactions demonstrated that hydrodynamic interactions do not play a significant role. At large strain amplitudes they found nonlinearities that agree well with the results of light scattering measurements [12] and with the Kinetic Chain Model [1].

II. SIMULATION METHOD

To study field-induced rheology we have extended the 3-D Brownian dynamics simulation method reported for structure formation in quiescent induced dipolar suspensions [13] to include steady shear flow. Particles are treated as essentially hard spheres with induced dipolar interactions, Stokes friction against the solvent, and Brownian motion. Hydrodynamic interactions are not included, so these simulations correspond to the so-called "free-draining" limit. The results presented here are obtained from a simulation method developed to predict the evolution of large, $N = 10,000$ particle

systems over short times. This method has time complexity $O(N)$, but gives coarsening results that are indistinguishable from a separate, more direct $O(N^2)$ simulation developed to predict the evolution of smaller systems over longer times. Cyclic boundary conditions are used in the x and y directions, and semi-hard boundaries (discussed below) were used normal to the z-axis, which is the direction of the applied field. Because image charges were not included, these simulations correspond more closely to magnetorheological fluids, but we doubt that image charges play a significant role in real systems - even though the image charges do eliminate the capping charge - because the role of defects appears to be much larger. The size of the simulations led to structures whose scale of coarseness was much smaller than the simulation volume, minimizing the effect of the cyclic boundary conditions.

A. Brownian dynamics

To describe our simulations we start with the equation of motion for the ith particle,

$$m\mathbf{a}_i = \mathbf{F}_h(\mathbf{v}_i) + \sum_{j \neq i} \mathbf{F}_{hs}(r_{ij}) + \sum_{j \neq i} \mathbf{F}_d(\mathbf{r}_{ij}) + \mathbf{F}_{bound}(z_i) + \mathbf{F}_B \qquad (1)$$

where $\mathbf{F}_h$ is the hydrodynamic Stokes force, $\mathbf{F}_{hs}$ is the quasi-hard sphere force, $\mathbf{F}_d$ is the dipolar force, $\mathbf{F}_{bound}$ is the interaction force of the particles with the bounding surfaces normal to the applied field, which is in the z direction, and $\mathbf{F}_B$ is the Brownian force, discussed below, and $\mathbf{r}_{ij}$ is the vector between the centers of spheres i and j.

The Stokes force on a sphere of radius a is $\mathbf{F}_h(\mathbf{v}_i) = -\varsigma(\mathbf{v}_i - \mathbf{v}_f)$, where $\mathbf{v}_f$ is the fluid velocity, $\mathbf{v}_i$ is the particle velocity, and the friction factor is $\varsigma = 6\pi\eta_o a$, assuming stick boundary conditions, with η_o the solvent viscosity. In steady shear the fluid velocity is $\mathbf{v}_f = z\dot{\gamma}\hat{\mathbf{x}}$. The particles are modeled as quasi-hard spheres, with a repulsive force

essentially dependent on the *gap* between particles, $F_{hs}(r_{ij}) = A/(r_{ij} - cd)^{\alpha}$, where d is the particle diameter and $\alpha = 6$ and $c = 0.97$ are constants. The parameter A is then chosen in order to give zero interaction force when two particles aligned along the z axis, and interacting with the dipolar force, are separated by $r_{ij} = d$. This choice of parameters gives a good compromise between run time and the precision by which particle boundaries are defined. For example, if one were to choose $c = 0.99$, and A accordingly, the particle boundaries would be slightly more precise, but the gradient of the force would be much larger at contact, which would require a smaller discrete time step. This parameter A depends on the magnitude of the dipolar interaction, so we will not specify it until we convert to a dimensionless equation.

In the point dipole approximation, [14] the potential of interaction between two polarizable spheres i and j whose line of centers makes an angle θ_{ij} to the applied field, and whose centers are separated by a distance r_{ij} is

$$V(\mathbf{r}_{ij}) = -\alpha \left(\frac{d}{r_{ij}} \right)^3 \left(3\cos^2\theta_{ij} - 1 \right). \qquad (2)$$

For dielectric particles in an electric field $\alpha = \frac{1}{8} p^2 / 4\pi a^3 \varepsilon_0 \kappa_c$ where the particle dipole moment is $\mathbf{p} = 4\pi a^3 \varepsilon_o \kappa_c \beta \mathbf{E}_0$, and the dielectric contrast factor is $\beta = (\kappa_p - \kappa_c)/(\kappa_p + 2\kappa_c)$ in terms of the dielectric constants of the particle and continuous (liquid) phases, and $\varepsilon_o = 8.854 \times 10^{-12}$ F/m is the vacuum permittivity [14]. Combining gives the standard result $\alpha = \frac{1}{2}\pi\varepsilon_0\varepsilon_c a^3 \beta^2 E_0^2$. For a suspension of spherical magnetic particles in a magnetic field, $\alpha = \frac{1}{8}\mu_0 \kappa_{\mu,c} m^2 / 4\pi a^3$. For magnetically soft particles the magnetic moment is $\mathbf{m} = 4\pi a^3 \beta_{\mu} \mathbf{H}_0$, in terms of the magnetic contrast factor is $\beta_{\mu} = (\kappa_{\mu,p} - \kappa_{\mu,c})/(\kappa_{\mu,p} + 2\kappa_{\mu,c})$, where $\kappa_{\mu,c}$ is the relative permeability (to the vacuum)

of the continuous (liquid) phase, $\kappa_{\mu,p}$ is the relative permeability of the particles, and $\mu_o = 4\pi\text{x}10^{-7}$ H/m is the vacuum permeability [14]. Combining these gives an expression analogous to the dielectric case, $\alpha = \frac{1}{2}\pi\mu_o\kappa_{\mu,c}a^3\beta_\mu^2 H_o^2$. (Note in the magnetic case that although the expression for α is perfectly analogous to the electric case, the expression for the magnetic dipole is not, due to the fact that the magnetization has the units of the magnetic field $\mathbf{H}$, whereas the polarization has the units of the displacement field $\mathbf{D}$.)

Differentiating the potential gives the interaction force

$$\mathbf{F}_d(\mathbf{r}_{ij}) = -\frac{f_c}{2}\left(\frac{d}{r}\right)^4\left[\left(3\cos^2\theta_{ij} - 1\right)\hat{r}_{ij} + \sin 2\theta_{ij}\,\hat{\theta}_{ij}\right]. \tag{3}$$

where f_c is the force at contact between two spheres aligned with the field. Note that although the radial component of the dipolar force is attractive only when $\theta < 54.7°$, the tangential component of the force will always lead to chaining in a system with finite noise. Here f_c is the interaction force between two particles, where $f_c = \frac{3}{2}\pi\varepsilon_o\kappa_c a^2\beta^2 E_o^2$ for dielectric particles and $f_c = \frac{3}{2}\pi\mu_o\kappa_{\mu,c}a^2\beta_\mu^2 H_o^2$ for magnetic particles.

The interaction force with the boundaries is intentionally weak to reduce the effect of finite simulation volume. This force increases linearly as the particle enters the electrode, e.g. at the lower boundary it is given by the relation $\mathbf{F}_{bound} = \alpha(1 - z_i/a)$ for $z_i \leq a$, where α is a stiffness parameter that is adjusted to be just large enough to prevent particles from passing through the boundary.

Finally, the fluctuating Brownian force is given by $\mathbf{F}_B(t) = f_B\mathbf{R}_\tau(t)$, where τ is the correlation time of this force, as described in Appendix A. This force gives a particle diffusion coefficient $D_t = (f_B/\zeta)^2\tau$, and the relationship of the Brownian term to the dimensionless parameter $\lambda = \frac{2}{3}af_c/k_BT$ will be described below.

B. Dimensionless units and temperature scale

Dropping the inertial term leads to a set of coupled Langevin equations that for steady shear can be expressed in terms of the dimensionless variables,

$$\frac{\partial \mathbf{r}_i'}{\partial t'} = 32 Mn z_i' \hat{\mathbf{x}} + \sum_{j \neq i} \mathbf{f}_{hs}(r_{ij}') + \sum_{j \neq i} \mathbf{f}_d(\mathbf{r}_{ij}') + \mathbf{f}_{bound}(z_i') + J' R_{\tau/\tau_1} \qquad (4)$$

The Mason number is defined as $Mn = \eta_0 \dot{\gamma} / 2\varepsilon_0 \kappa_c \beta^2 E_0^2$ for a suspension of dielectric particles and as $Mn = \eta_0 \dot{\gamma} / 2\mu_0 \kappa_{\mu,c} \beta_\mu^2 H_0^2$ for a suspension of magnetic particles. The spatial variables are normalized such that the particle diameter is unity, $r' = r/d$, and the time variable $t' = t/\tau_1$ is normalized by the characteristic time $\tau_1 = 32 Mn/\dot{\gamma}$, which is independent of particle size. This choice of normalized variables gives $\mathbf{f}_d(\mathbf{r}_{ij}') = -r_{ij}'^{-4}\left[\left(3cos^2\theta_{ij} - 1\right)\hat{r}_{ij} + sin2\theta_{ij}\hat{\theta}_{ij}\right]$. The dimensionless hard sphere force for the uniaxial case is given by $\mathbf{f}_{hs}(r_{ij}') = 3.0 \times 10^{-9} / \left(r_{ij}' - 0.97\right)^6$, and the boundary force at the lower boundary is given by $\mathbf{f}_{bound} = \alpha'\left(1 - z_i'\right)$ for $z_i' \leq 1/2$ where dimensionless stiffness parameters of $\alpha' \sim 10.0$ prevent particles from escaping the simulation volume, yet are soft enough to reduce finite size effects.

The dimensionless time we use is $\Delta t' = \Delta t / \tau_1$. For the electric field case $\tau_1 = \varepsilon_o \kappa_c \beta^2 E_o^2 / 16\eta_o$ which for a viscosity of 1.0 cp, an applied field of 1.0 kV/mm, and $\kappa_c \beta^2 = 2$, $\tau_1 \approx 10^{-3} s$, so one dimensionless time unit is about a millisecond. For the magnetic field case the dimensionless time is $\tau_1 = 16\eta_o / \mu_o \kappa_{\mu,c} \beta_\mu^2 H_o^2$. For a suspending liquid with a viscosity of 1 cp, an applied field of $H_o = 3.58$ A/m (45 Oe), $\mu_c = 1$ and $\beta_\mu = 1$ one dimensionless time unit is the same, about a millisecond. Throughout this paper we use the convention that one dimensionless time unit is 1.0 ms.

7

In Eq. 4 the Brownian motion enters as $J'R_{\tau/\tau_1}$, where the dimensionless constant $J' = 2f_B/f_c$. In terms of the dimensionless parameter $\lambda = \frac{2}{3}af_c/k_BT$ the dimensionless thermal force is thus $J' = 4\lambda^{-1}\sqrt{2\tau_D/3\tau}$ where the characteristic diffusion time is $\tau_D = a^2/6D_t$. Using the easily derived relation $\tau_D/\tau = \frac{1}{24}J'^{-2}(\tau_1/\tau)^2$ then gives $\lambda = \frac{2}{3}J'^{-2}(\tau_1/\tau)$. To remove the effect of the correlation time on temperature we define the parameter $J = J'/\sqrt{\tau/\tau_1}$ to obtain $\lambda = \frac{2}{3}J^{-2}$. The simulations we report are over the range J=0.10-0.45, which thus corresponds to the range λ=66.7 - 3.3.

In our simulation method we drop the effect of particle inertia, which raises the issue of determining over what regime of particle sizes we can expect this approximation to be correct. When a suspended particle in a fluid is acted upon by an constant external force, the time needed for the particle to accelerate to a fixed terminal velocity is $t_0 = m/6\pi a\eta_0$, where m is the particle mass; in terms of the particle density ρ this time is $t_0 = 2\rho a^2/9\eta_0$. For an ER fluid consisting of 1 μm diameter particles of density 2.5 g/cm³, in a suspending fluid with a viscosity of 1.0×10^{-2} poise, this acceleration time is $t_0 = 0.14$ μs. Now consider how far a particle might move, relative to its own diameter, in this time. The terminal velocity of the particle is obtained by balancing the electrostatic force acting on it by the hydrodynamic drag. The electrostatic force between two particles is at a maximum when the two particles are in contact along the z axis, and in this case $f_c = \frac{3}{2}\pi\varepsilon_0\kappa_c a^2\beta^2E_0^2$. The distance Δz a particle under this force can travel in the time t_0 is $\Delta z/2a = (f_c/12\pi a^2\eta_0)t_0$. In an applied field of 1.0 kV/mm, with $\kappa_c\beta^2 = 2$, we obtain $\Delta z/2a = 1.5\times10^{-4}$. Thus in this circumstance the particle has reached terminal velocity after moving only 0.015% of its diameter, and inertia can be safely ignored. Because $\Delta z/2a \propto \rho(aE_0/\eta_0)^2$ inertial effects can become significant for very large, dense particles, exposed to large fields in a low viscosity fluid, such as can occur in MR fluids.

C. Fluid stress

A simple argument for the fluid stress is as follows [15]. Let $\mathbf{v}_k^0$ be the unperturbed velocity of the fluid at the location of the k-th particle. The work done per unit time by the fluid on this particle is $w_k = -\mathbf{F}_k \cdot \mathbf{v}_k^0$. The increase in energy loss per unit time is, per unit volume, $w = \left(3\phi/4\pi a^3\right)\langle -\mathbf{F}_k \cdot \mathbf{v}_k^0 \rangle$. In simple shear the unperturbed fluid velocity field is given by $\mathbf{v}^0 = \dot{\gamma}z\hat{x}$ so $w = \left(3\phi\dot{\gamma}/4\pi a^3\right)\langle -F_{x,k}z_k \rangle$. To relate this energy dissipation per unit volume to the suspension viscosity consider two parallel plates of area A separated by a distance h are moving relative to each other at a shear velocity $|\mathbf{v}| = \dot{\gamma}h$. The frictional force on the moving plate is $F = \eta\dot{\gamma}A$ and the total work per unit time on the volume hA is $F|\mathbf{v}| = \eta\dot{\gamma}^2 hA$. Thus the excess work per unit volume due to the particles is $w = \left(\eta - \eta_0\right)\dot{\gamma}^2 = \Delta\sigma\dot{\gamma}$, which combined with the above expression for the work gives the expression for the excess stress $\Delta\sigma = \left(3\phi/4\pi a^3\right)\langle -F_{x,k}z_k \rangle$. In terms of the normalized coordinates in Eq. 4, the stress is

$$\Delta\sigma = \left(3\phi f_c/4\pi a^2\right)\langle -f_{x,k}z_k' \rangle, \tag{5}$$

which is independent of particle size. The dimensionless *field-specific viscosity* [1] is

$$\eta_f \equiv (\eta - \eta_\phi)/\phi\eta_0 = \tfrac{9}{16}Mn^{-1}\langle -f_{x,k}z_k' \rangle, \tag{6}$$

which is the relative viscosity increase due to the applied field per unit volume fraction of particles, with $\eta_\phi \cong \eta_0(1 + 2.5\phi)$ the Einstein viscosity of a particle suspension.

RESULTS

Simulations in steady shear were done by first allowing the suspension to structure for 25 ms in the field without shear. The shear was then turned on at the maximum Mason number and held for 25 ms. The Mason number was then progressively reduced over the next 950 ms to explore a range of Mn, and the stress was computed every 0.1 ms.

Results of steady shear simulations in a uniaxial field are shown in **Fig. 1** for a 30 vol.% solution and show that the stress is essentially independent of Mason number over the range investigated in the absence of Brownian motion, indicating the expected shear thinning viscosity $\eta_F \sim Mn^{-1}$. In the dimensionless units of this plot, the stress is about 0.25, which is somewhat lower than one would expect from the chain model, where this amplitude would be about 0.5-1.0, depending on whether polydispersity is taken into account. (In these simulations the stress per unit particle concentration is essentially constant until $\phi=40$ vol.%, whereupon it decreases with concentration.) As Brownian motion is introduced the stress decreases at low Mason number, with the apparently logarithmic dependence $\Delta\sigma = \Delta\sigma_0[1 + c_0 \ln c_1 Mn]$ in the region where a dependence on Mn is observed. This will cause the apparent shear thinning exponent b of the field-specific viscosity $\eta_F \sim Mn^{-b}$ to be significantly less than 1, perhaps accounting for the trends seen in experimental data, where values as small as $b \cong 2/3$ are found [6]. In fact, it was suggested in these studies that the small exponents were due to the importance of λ, and the simulations of Melrose [5], Guo [7] and Baxter-Drayton and Brady [9] have concluded this as well. In the following we present a detailed model of thermal fluctuations, based on chain dynamics.

A prominent feature of these simulations is the emergence of a striped phase [2-5,7] at large λ and at concentrations up to 40 vol.%, **Fig. 2**. These sheet-like structures are in the plane of the field and flow direction, i.e. orthogonal to the axis of fluid vorticity, and have also been observed experimentally [16]. At small λ this phase is not observed, even

10

when there is substantial fluid stress. The thermal effects in these simulations are undoubtedly very complex, but the striped phase seems to consist of a sheets of dense chains, so in the discussion below we will simply ignore the overwhelming structural complexities and attempt to gain some insight into why the thermal effects are greatest at the lowest Mason numbers by considering a simplified chain model, justified in part by the fact that the striped phase only exists at high λ, where thermal effects are not strong.

DISCUSSION

To obtain an understanding of the effect of thermal fluctuations, we consider the elementary model of a chain of particles in shear flow, a description that is quite reasonable given that the striped phase does not form when thermal effects are strong. Rather than attempt to develop an accurate description of thermal fluctuations, with the associated algebraic complexities, we focus on the simple case of induced point dipoles and Stokes friction against the solvent. Local field effects, multipolar interactions, and hydrodynamic interactions, though useful in developing a quantitative model, are not included, since we do not believe they will change the conceptual description we present.

A. Athermal chain model

A few basic aspects of athermal chains [1] must be reviewed. We are specifically interested in computing the tension in the chain as well as the "bond" angle relative to the applied field along the contour length of a chain. This problem should be solved self-consistently, but an iterative method, which starts with a straight chain, is quite accurate.

Consider an initially linear chain of $2N+1$ spheres, numbered from $-N$ to N, in steady state (zero velocity) inclined at an angle θ_0 to the applied field. The shear flow is in the x direction, and the fluid velocity at position z is given by $\mathbf{v}_f = z\dot{\gamma}\hat{\mathbf{x}}$. The hydrodynamic

11

drag on each particle is $\mathbf{f}_s = \varsigma \mathbf{v}_f$ where assuming stick boundary conditions on the particles, the friction factor is $\varsigma = 6\pi\eta_0 a$, with η_0 the solvent viscosity and a the particle radius. The hydrodynamically induced tension in the chain between particles $i+1$ and i is

$$t_i = \sum_{k=i+1}^{N} \mathbf{f}_{s,k} \cdot \hat{\mathbf{r}}_i \approx 6\pi\eta_0 a^2 \dot{\gamma} \sin\theta_i \cos\theta_0 \left(N^2 - i^2\right) \tag{7}$$

The Stokes friction will also introduce a force tangential to the chain, of magnitude

$$s_i = \sum_{k=i+1}^{N} \mathbf{f}_{s,k} \cdot \hat{\boldsymbol{\theta}}_i \approx 6\pi\eta_0 a^2 \dot{\gamma} \cos\theta_i \cos\theta_0 \left(N^2 - i^2\right) \tag{8}$$

which also has a strong maximum near the chain center. To determine the chain angle in the absence of thermal fluctuations these forces are balanced against the dipolar forces.

The angle at the chain center can be computed by balancing the tangential hydrodynamic forces with the tangential dipolar force in Eq. 3.

$$\tan\theta_0 = 8MnN^2 \tag{9}$$

The variation of the chain angle along its contour length is also obtained by a force balance, with the first-order result

$$\sin\theta_i = \sin\theta_0 \left(1 - i^2/N^2\right) \tag{10}$$

Finally, to insure chain stability the radial component of the dipolar force must exceed the hydrodynamically induced tension, which at the chain center gives the maximum chain angle

$$\tan\theta_c = \sqrt{2/3} \qquad\qquad (11)$$

A chain at this tilt angle we call a critical chain, since it is at the brink of failure, and its length is given by $2N \approx (\sqrt{6}Mn)^{-1/2}$.

At fixed Mason number, and ignoring thermal fluctuations, the chain length will increase until the maximum tilt angle is attained, at which point further growth will cause the chain to break at the center, where the tensile forces are a maximum. The presence of chains increases the stress in the fluid by an amount that is approximately the torque density in the fluid, as can be shown from Eq. 5, if one uses $\tan\theta = 16MnN^2/3$, which insures that the field-induced torque balances the hydrodynamic torque (Appendix B)

$$\Delta\sigma = (3\phi f_c/2\pi a^2)\tan\theta\cos^2\theta \qquad\qquad (12)$$

In an athermal system one can expect that the system will evolve to a steady state where chains aggregate to their maximum stable length, attain the critical angle of Eq. 11, then fragment by breaking in the middle, to form chains of half maximum length that tilt at an angle that is roughly 1/4 of the maximum, then reaggregate, etc.

B. Fluctuation-induced fragmentation

The above description ignores the effect of thermal fluctuations, with the result that the chains are assumed to have an infinite lifetime if they are beneath their critical angle. In reality, chains will fragment, due to the combined effects of shear and thermal fluctuations. At low particle concentrations, where the collision processes that allow chains to form have long collision times, one would expect that thermal fluctuations would start to prevent the formation of critical chains when the lifetime of a chain

13

becomes significantly shorter than the time it takes to create a critical chain athermally. If the suspension is reasonably concentrated, these collision times become very short, and the rate limiting step for the generation of a critical chain, and thus stress, is the time it takes a chain to reach its maximum angle of inclination relative to the applied field, which is roughly the reciprocal shear rate $\dot{\gamma}^{-1}$. For such concentrated suspensions we thus invoke the stipulation that a chain cannot contribute fully to the fluid stress unless its thermal lifetime τ is greater than the reciprocal shear rate of the solution:

$$\tau\dot{\gamma} \geq 1. \tag{13}$$

This condition is reasonable because of the strong, quadratic dependence of the chain angle on the chain length, Eq. 9: when two half chains aggregate, they are at a very small angle relative to their maximum angle, and it will take a time proportional to $\dot{\gamma}^{-1}$ for this rotation to occur. Still, we will ultimately find it necessary to modify this relation.

Thermal fluctuations can cause a chain to break anywhere along its length. If a chain fragments between nodes i and $i+1$ it will break into two pieces, one of size $N-i$ and one of size roughly $N+i$. The rate at which the remaining larger chain loses the smaller fragment of size $N-i$ we call Γ_i. The mass-weighted overall fragmentation rate is then

$$\Gamma = 2\sum_{i=0}^{N-1} \frac{N-i}{N}\Gamma_i \tag{14}$$

The fragmentation rates are then just given by the inverse thermal lifetimes, $\Gamma_i = \tau_i^{-1}$, where we expect a standard activation process to determine the lifetime

$$\tau_i = \tau_{0,i}\exp(\Delta V_i / k_B T). \tag{15}$$

14

The computation of the activation energy ΔV_i will be pursued below. The prefactor $\tau_{0,i}$ can be estimated as the time it takes the two chain fragments to diffuse away from each other by a distance of roughly the particle radius a, $\tau_{0,i} \approx a^2/6D_{s,i}$, where the diffusion coefficient $D_{s,i} = D_{N-i} + D_{N+i}$ is the sum of the diffusion coefficients of the fragments. Summing the Stokes friction along the chain, without hydrodynamic interactions, gives

$$D_{N-i} + D_{N+i} = \left(k_B T/\varsigma\right)\left[(N-i)^{-1} + (N+i)^{-1}\right] = 2D_t N/(N^2 - i^2),$$ where D_t is the diffusion coefficient of a particle. Again calling the time it takes a particle to diffuse its own radius $\tau_D \approx (a^2/6D_t) = (\pi\eta_0 a^3/k_B T)$ we obtain the chain lifetime

$$\tau = \tau_D \left[\frac{4}{N}\sum_{i=0}^{N-1}\left(\frac{1-i/N}{1-i^2/N^2}\right)\exp(-\Delta V_i/k_B T)\right]^{-1} \tag{16}$$

In terms of the Peclet, number $Pe = 3\pi\eta_0 a^3 \dot{\gamma}/k_B T = 6\lambda Mn$

$$\dot{\gamma}\tau_D = \tfrac{1}{3}Pe \tag{17}$$

To make further progress in this model of parallel decay channels, we must estimate the activation energies along the chain.

C. Activation energies

Rather than laboring to determine the potential energy surface of a chain in shear, we shall consider two elementary rupture mechanisms - tensile and shear - and simply take the lowest activation energy. Implicit in the following is a subtle point: because the prefactors in Eq. 15 are just the chain rotational diffusion times, which are also the longest relaxation times of the chain, we shall assume that outside the perturbations we

consider, the chain has had time to come to mechanical equilibrium.

Radial fluctuation -- In a tensile break the energy required is that energy needed to separate the particles sufficiently such that the radial component of their dipolar interaction force equals the tension on the chain [1]. The chain will then rupture because the negative curvature of the dipolar interaction insures that the interaction force monotonically decreases with separation, allowing the hydrodynamic tension to pull the chain apart. The chain tension at particle i, Eq. 7, is exactly balanced by the radial dipolar force, Eq. 3, at a particle separation we call r^*, and it is readily shown, using Eqs. 9&10, that

$$\frac{d}{r_i^*} = \sqrt[4]{\frac{\sin^2\theta_i}{1 - \frac{3}{2}\sin^2\theta_i}} \qquad (18)$$

This result gives $r^* = d$ when $\tan\theta_i = \sqrt{2/3}$, so that when the center of the chain is at its critical angle it will rupture at contact, just as it should. And as the chain angle decreases to zero, rupture will occur only at infinite separation, since in this case the hydrodynamic tension is zero. The reduced activation energy for this rupture mode is then

$$\Delta V_i / k_B T = \left[V(r_i^*) - V(d)\right]/k_B T = \frac{1}{2}\lambda\left(3\cos^2\theta_i - 1\right)\left\{1 - \left[\sin^2\theta_i \big/\left(1 - \frac{3}{2}\sin^2\theta_i\right)\right]^{3/4}\right\} \qquad (19)$$

and the maximum value is λ.

Tangential fluctuation -- A tangential fluctuation will cause chain fragmentation if the fluctuation causes the radial component of the dipolar force to be less than the hydrodynamic tension. Balancing the chain tension, Eq. 7, with the radial component of the dipolar force, Eq. 3, gives an expression for the rupture angle θ_i^*

16

$$\left(3\cos^2\theta_i* - 1\right)\big/\sin\theta_i* = 2\sin\theta_{e,i} \qquad (20)$$

where $\theta_{e,i}$ is the unperturbed chain angle at the i-th particle, given from Eqs. 9&10 by the relation $\sin\theta_{e,i} = 8Mn(N^2 - i^2)\cos\theta_0$. If the chain is near its critical angle then $\cos^2\theta_i* = 3/5$, whereas if the chain angle is near zero then $\cos^2\theta_i* = 1/3$. The reduced activation energy for this fluctuation is

$$\Delta V_i/k_B T = \left[V(d,\theta_i*) - V(d,\theta_i)\right]\big/k_B T = \tfrac{3}{2}\lambda\left(\cos^2\theta_{e,i} - \cos^2\theta_i*\right) \qquad (21)$$

and is actually comparable to, but somewhat smaller than, the reduced radial fluctuation activation energy, Eq. 19, again having a maximum value of λ.

To proceed, we note, **Fig. 3**, that a direct comparison shows that these complex expressions for the fragmentation activation energies are very closely approximated by the simple expression

$$\Delta V_i/k_B T = \lambda\left(1 - \tan\theta_{e,i}/\tan\theta_c\right) \approx \lambda\left[1 - \left(\tan\theta_e/\tan\theta_c\right)\left(1 - i^2/N^2\right)\right] \qquad (22)$$

where θ_e is the *equilibrium chain angle at the chain center*, in the presence of thermal fluctuations and shear, and is the quantity that we now wish to obtain.

D. Chain angle and size

The chain angle and size can now be obtained. Substituting Eq. 22 into Eq. 17 gives

$$\tau = \frac{\tau_D}{\Omega}\exp\left[\lambda\left(1 - \tan\theta_e/\tan\theta_c\right)\right] \qquad (23)$$

17

where we have passed to the continuum limit to obtain the integral

$$\Omega = 4\int_0^1 \frac{1}{1+\sigma}\exp\left(-\sigma^2\lambda\tan\theta_e/\tan\theta_c\right)d\sigma.\tag{24}$$

Using the condition in Eq. 13, we obtain, with Eq. 17

$$\tan\theta_e/\tan\theta_c = 1 + \lambda^{-1}\ln\left(Pe/3\Omega\right)\tag{25a}$$

$$N_e = N_c\sqrt{\tan\theta_e/\tan\theta_c}\tag{25b}$$

An exact analytical solution to Eqs. 24&24 is not apparent, but asymptotic and iterative solutions to this problem are possible. It is helpful that Ω appears in the logarithm.

Small λ -- For small $\lambda, \Omega \approx 2.75 - 0.75\lambda\tan\theta_e/\tan\theta_c$. To zero-th order

$$\tan\theta_e/\tan\theta_c = 1 + \lambda^{-1}\ln(\alpha Pe)\tag{26}$$

where the parameter $\alpha \approx 1/8$ in our calculation, but really should be treated as a free parameter, since we have used several estimates in obtaining this, including Eq. 13. Note that this approximation is only valid when $\lambda + \ln(\alpha Pe) \ll 1$. This severe constraint limits the practical utility of this result to very small λ, where it is doubtful that an ER or MR effect occurs.

Large λ -- For large λ we make the approximation that the chain angle will be close to the critical angle for reasonable Mason numbers, giving

$$\Omega = 4\int_0^1 \frac{1}{1+\sigma}\exp\left(-\sigma^2\lambda\right)d\sigma \approx \sqrt{4\pi/\lambda}\tag{27}$$

$$\tan\theta_e/\tan\theta_c = 1 + \lambda^{-1}\ln\left(\tfrac{1}{6}Pe\sqrt{\lambda/\pi}\right) = 1 + \lambda^{-1}\ln\left(Mn\sqrt{\lambda^3/\pi}\right). \qquad (28)$$

This solution is surprisingly accurate, as we shall demonstrate, but one should note that for the purpose of comparison to experimental data, an adjustable parameter should be put into the log. Note that the simple dependence on the Peclet number in Eq. 26 is significantly altered.

Iterative solution -- It is possible to solve Eqs. 24-25 numerically, but this would require solving the integral in Eq. 24 a tremendous number of times. A better approach is to use the approximation, which is exact for $\rho \equiv \lambda\tan\theta_e/\tan\theta_c \gg 1$,

$$\Omega = 4\int_0^1 \frac{1}{1+\sigma}\exp\left(-\sigma^2\rho\right)d\sigma \approx 4\int_0^1 \exp\left(-\sigma^2\rho\right)d\sigma \approx 4/\sqrt[4]{1+(4\rho/\pi)^2}. \qquad (29)$$

This numerical approximation is really better than it looks, because the factor dropped from the integral decreases roughly linearly from 1.0 to 0.5 on the interval [0,1], and becomes completely unimportant when $\rho \gg 1$. Solving Eqs. 25a&29 iteratively shows that Eq. 28 is a good approximation.

Limits -- We first note that the ER/MR effect, within the context of the chain model, only occurs for Mason numbers smaller than $Mn^* = \tfrac{1}{8}\sqrt{2/3} \approx 0.1$. Then note that our two approximate solutions, Eqs. 26&28, are identical when $\lambda \approx 1.77$. Eq. 29 indicates that the ER/MR effects become negligible when $1 + \lambda^{-1}\ln\left(Mn^*\sqrt{\lambda^3/\pi}\right) = 0$, that is $\lambda \approx 1.9$. Eq. 26 at best has a very restricted domain of utility, and we will now focus on Eq. 28.

One can expect to observe a field-induced rheology that is not reduced by thermal fluctuations when

$$\sqrt{\pi/\lambda^3} \le Mn \le Mn* \qquad (30)$$

A full ER/MR effect is possible when these limits are equal, $\lambda \approx 6.7$. Eq. 30 seems counter-intuitive, because it shows that the regime where temperature plays no role is quite modest, even for reasonable values of λ. The regime where an ER/MR effect can be observed, but is affected by thermal fluctuations, is

$$\sqrt{\pi/\lambda^3} \times e^{-\lambda} \le Mn \le Min\left(\sqrt{\pi/\lambda^3}, Mn*\right) \qquad (31)$$

This range of Mn can be quite large for large λ, making the slope of the thermal effect difficult to measure. For large λ the slope of the thermal effect will be so small as to be unobservable. Let us suppose an experimental criterion of at least a 10% change in stress per decade change in Mn. Roughly speaking, Eq. 31 shows the range of the ER/MR effect to be over $\lambda/2.3$ decades of Mn. Thus our criterion is $2.3/\lambda \ge 0.1$, or $\lambda \le 23$.

E. Self-consistent model

The simple description we have presented is not self-consistent, because Eq. 13 stipulates that the thermal lifetime be independent of the equilibrium chain angle. The self-consistent condition is

$$\tau\dot{\gamma} \approx \tan\theta_e \qquad (32)$$

whereupon Eq. 25a becomes the transcendental equation

$$\tan\theta_e/\tan\theta_c + \lambda^{-1}\ln\left(\tan\theta_e/\tan\theta_c\right) = 1 + \lambda^{-1}\ln\left(\tfrac{1}{3}Pe/\Omega\tan\theta_c\right) \qquad (33)$$

and Ω is still given by Eq. 29. An immediate consequence of this is that when $\lambda\tan\theta_e \ll \tan\theta_c$, the relationship $\tan\theta_e \propto Pe\times\exp(\lambda)$ obtains, using Eq. 26. (Thus at very low Mn the viscosity is proportional to $\eta_F \propto \lambda\exp(\lambda)$.) This linear in Mn relationship is followed by a logarithmic dependence of the chain angle on Mn, as before. The effect of this self-consistency on the $\tan\theta_e$ curves is quite significant, as shown in **Fig. 4**. The largest changes occur at small λ, which is where experiments will most readily detect thermal effects. To some extent, this condition of self-consistency is problematic; when the equilibrium chain angle becomes very small, the lifetime in Eq. 32 will be much shorter than the chain collision times, so that chains will not form in the first place. From primitive considerations of shear-driven aggregation we deduce that the chain collision time is of order $\tau\dot{\gamma}\approx\phi^{-1}$, suggesting that using the self-consistency condition at low chain angles might not be appropriate.

F. Comparison to simulations

The Thermal Chain Model does a good job of predicting the trends seen in **Fig. 1**, including the logarithmic dependence on Mn. A parameter-free collapse of all the simulation data on axes suggested by Eq. 28 is also reasonably successful, as shown in **Fig. 5**. To scrutinize the agreement in further detail would require the compilation of more simulation data, to obtain better statistics. Still, it must be emphasized that a complete description of thermal effects should address the issue of the chain growth kinetics.

CONCLUSIONS

In steady shear a striped phase readily forms for large λ, and when Mn is large. For small λ, the striped phase does not form, even at the highest Mn. For $\lambda \sim 15$ a striped phase only forms at the highest Mn. The effect of thermal fluctuations on the uniaxial field-induced rheology is essentially logarithmic in Mn, and can be accounted for by the Thermal Chain Model.

APPENDIX A: Correlated thermal fluctuations

There are a number of problems in implementing Brownian motion into a simulation where one is integrating a first order differential equation, so a description of how we chose to do this is useful. This is not the only possible approach, but it is a method that allows one to mimic the effect of particle inertia without resorting to a second order differential equation.

The equation of motion of a Brownian particle is [17]

$$m\dot{\mathbf{v}} = -\zeta \mathbf{v} + \mathbf{F}_B(t), \tag{A.1}$$

where $\mathbf{v}$ is the particle velocity, m is the particle mass, and $\zeta = 6\pi\eta_o a$ is the friction coefficient of a particle of radius a against a liquid of viscosity μ_0. $\mathbf{F}_B(t)$ is a stochastic force that is normally considered to have a time correlation function that is a delta function. The time correlation function of the diffusing particle is [17]

$$\langle \mathbf{v}(0) \cdot \mathbf{v}(t) \rangle = (3k_B T/m)\exp(-t/\tau) \tag{A.2}$$

where the relaxation time is $\tau = m/\zeta$. Using the Kubo relation [17]

$$D_t = \tfrac{1}{3} \int\limits_0^\infty \langle \mathbf{v}(0) \cdot \mathbf{v}(t) \rangle dt \qquad\qquad (A.3)$$

then gives the Stokes-Einstein relation for the translational diffusion coefficient $D_t = k_B T / \zeta$. Thus it is the persistence of motion of a particle acted upon by a uncorrelated stochastic force that is responsible for a finite diffusion coefficient. In some sense the situation is subtle; the diffusion coefficient of a particle is independent of the particle mass, yet the relaxation time is proportional to the mass, and the amplitude of the velocity autocorrelation function is inversely proportional to the mass.

The relaxation time for a 1 μm diameter silica sphere in water is 5.5×10^{-7} s, but we would expect an applied field of 1.0 kV/mm to structure silica spheres in such a solution on millisecond time scales. In our simulations we set the discrete time step to a maximum of 2.0×10^{-5} s, so the natural time scale for Brownian motion is much faster than the time scales we wish to investigate. A completely physical simulation of field-induced rheology with Brownian motion is not feasible and a practical method is needed.

We start with the first order differential equation $\zeta \mathbf{v} = \mathbf{F}_B(t)$, obtained by dropping the inertial term. If $\mathbf{F}_B(t)$ is considered to be a stochastic force with a delta function time correlation function, then the diffusion coefficient of a particle will now depend on the discrete time step used to solve the equation. For example, consider the simple one dimensional case where $F_B(t) = f_B s_i$, and s_i is a simple uncorrelated random variable that is either ± 1 during the i-th time step. Then during the time Δt the particle will move a distance $\Delta x = (f_B / \zeta) \Delta t$. Over a total time t the number of steps will be $N = t / \Delta t$ and from the theory of random walks the mean square displacement will be $< x^2 >= N \Delta x^2 = (f_B / \zeta)^2 \Delta t \cdot t$. Thus the diffusion coefficient $D_t = \tfrac{1}{2}(f_B / \zeta)^2 \Delta t$ has an unphysical dependence on the discrete time step. A simple way to handle this is to scale the amplitude of the Brownian force by $f_B \propto \Delta t^{-1/2}$. However, because the time step is

allowed to vary in our simulation method, this can lead to divergent force amplitudes that can potentially create stability problems when two "hard" spheres are nearly in contact.

To avoid stability problems we have taken a different approach. Let us write the Brownian force as $\mathbf{F}_B(t) = f_B \mathbf{R}_\tau(t)$ where $\mathbf{R}_\tau(t)$ is a time-correlated random variable whose autocorrelation function has a decay time τ. Using the Kubo relation we then have $D_t = \left(f_B/\zeta\right)^2 \int_0^\infty < R_{\tau,x}(0) R_{\tau,x}(t) > dt$ where we have used the isotropy of space to obtain $< \mathbf{R}_\tau(0) \cdot \mathbf{R}_\tau(t) >= 3 < R_{\tau,x}(0) R_{\tau,x}(t) >$. If our time correlated variable is normalized such that $< R_{\tau,x}(0) R_{\tau,x}(0) >= 1$, then the relaxation time is $\tau = \int_0^\infty < R_{\tau,x}(0) R_{\tau,x}(t) > dt$, and $D_t = \left(f_B/\zeta\right)^2 \tau$. The amplitude of the Brownian force is now $f_B^2 = k_B T \zeta / \tau$, and so can be controlled by a judicious selection of τ.

To construct the correlated random variable we start with the primitive uncorrelated random variable s_i, with $<s_i s_j> = \delta_{ij}$. Define the function $\Gamma_i = (1-\varepsilon)\Gamma_{i-1} + \varepsilon s_i$ and note that by a straightforward calculation the exponential correlation $< \Gamma_i \Gamma_{i+k} >= \left[\varepsilon/(2-\varepsilon)\right](1-\varepsilon)^k$ is obtained. If we let $R_i = \Gamma_i \sqrt{(2-\varepsilon)/\varepsilon}$ then $< R_i R_{i+k} >= (1-\varepsilon)^k$ and $\tau \approx \varepsilon^{-1}$. In practice, the correlation time is chosen to be larger than the maximum discrete time step of 2 µs, but smaller than the ms time scale of structural evolution. We chose 10 µs, so on times scales short compared to this ballistic motion occurs and the effect of particle inertia on diffusion is obtained without resorting to a second-order differential equation.

APPENDIX B: Stress in the chain model

The use of Eq. 5 to compute the stress of a chain is sufficiently subtle as to warrant clarification. It is often a convenient simplification to represent a chain as linear, with nearest neighbor dipole interactions. But if this is done, one can easily show that the

dipolar force on the i-th particle, which is the sum of the dipolar forces due to its nearby neighbors, is zero. Thus the quantity in the brackets is thus apparently zero in this linear approximation. This dire situation can be remedied by lumping the two particle forces - the dipolar and hard sphere - into a single total force acting on the i-th particle, $\mathbf{F}_i$. This force is due to the interactions with both neighbors. Because inertia is negligible, this force is exactly balanced by the Stokes friction against the solvent, $\mathbf{F}_i - \varsigma(\mathbf{v}_i - \mathbf{v}_f) = 0$. For a stationary chain the particle velocity is zero and $\mathbf{F}_i = -\varsigma \mathbf{v}_f$. To counterbalance this force a real chain simply must have curvature, so that the tangential dipolar interactions caused by its neighbors are not equal and opposite: an initially linear chain in shear flow will simply deform until it assumes the shape closely given by Eq. 10.

This problem is avoided by simply using the supposition that the chain is stationary, then for any chain shape easily use Eq. 5 or its dimensioned equivalent, to compute the stress with $\mathbf{F}_i = -\varsigma \mathbf{v}_f$. Using $z_k = 2a\cos\theta$ Eq. 5 becomes

$$\Delta\sigma = 18\phi\eta_0\dot{\gamma}\cos^2\theta\langle k^2\rangle \tag{B.1}$$

Then the relation $\langle k^2\rangle = N^{-1}\sum_{k=1}^{N}k^2 \approx \frac{1}{3}N^2$ is used, which along with the result $\tan\theta = \frac{16}{3}MnN^2$, gives Eq. 12, which in electrostatic units is the result $\Delta\sigma = \frac{9}{8}\phi\varepsilon_o\kappa_c\beta^2E_0^2\sin2\theta$ published in our 1996 paper [1]. (This expression for the chain angle is not the same as Eq. 9, which is for the central angle of a curved chain, the distinction being that $\tan\theta = \frac{16}{3}MnN^2$ insures that the hydrodynamic and electrostatic torques balance for a rigid chain). A careful thinker will note that at the central particle in a real chain with an odd number of particles, the dipolar and hard sphere forces exactly balance. This implies that this particle must move at the fluid velocity at that point, which is of course correct.

REFERENCES

1. J. E. Martin and R. A. Anderson, *J. Chem. Phys.* **104**, 4814-4827 (1996).

2. M. Whittle, *J. Non-Newtonian Fluid Mech.* **37**, 223-263 (1990).

3. J. R. Melrose, *Phys. Rev. A* **44**, R4789-R4792 (1991).

4. J. R. Melrose, *Mol. Phys.* **76**, 635-660 (1992).

5. J. R. Melrose and D. M. Heyes, *J. Chem. Phys.* **98**, 5873-5886 (1993).

6. T. C. Halsey, J. E. Martin and D. Adolf, *Phys. Rev. Lett.* **68**, 1519-1522 (1992).

7. H. X. Guo, Z. H. Mai and H. H. Tian, *Phys. Rev. E* **53**, 3823-3831 (1996).

8. R. T. Bonnecaze and J. F. Brady, *J. Chem. Phys.* **96**, 2183-2202 (1992).

9. Y. Baxter-Drayton and J. F. Brady, *J. Rheol.* **40**, 1027-1056 (1996).

10. M. Parthasarathy and D. J. Klingenberg, *Rheol. Acta.* **34**, 417-429 (1995).

11. M. Parthasarathy and D. J. Klingenberg, *J. Non-Newtonian Fluid Mech.* **81**, 83-104 (1999).

12. J. E. Martin and J. Odinek, *Phys. Rev. Lett.* **75**, 2827-2830 (1995); J. E. Martin and J. Odinek, *J. Rheol.* **39**, 995-1009 (1995).

13. J. E. Martin, R. A. Anderson and C. P. Tigges *J. Chem. Phys.* **108**, 3765-3787 (1998).

14. J. R. Reitz and F. J. Milford, *Foundations of Electromagnetic Theory* (Addison Wesley, Reading, MA, 1967).

15. H. Yamakawa , *Modern Theory of Polymer Solutions* pp. 258-259 (Harper & Row, New York, 1971).

16. O. Volkova, S. Cutillas, and G. Bossis, *Phys. Rev. Lett.* **82**, 233-236 (1999); O. Volkova, S. Cutillas, P. Carletto, G. Bossis, A. Cebers, A. Meunier, *J. Magnetism and Magnetic Materials* **201**, 66-69 (1999).

17. B. Berne and R. Pecora, *Dynamic Light Scattering,* pp. 83 (Wiley & Sons, New York, 1976).

FIGURE CAPTIONS

1. Shear simulations in a uniaxial field at $\phi=30\%$ show the stress is nearly independent of Mn for $\lambda=\infty$, indicating a shear thinning viscosity. Brownian motion decreases the stress significantly at low Mn.

2. A striped phase emerges at large λ, but not at small λ. These structures are at the marginal value $\lambda=16.7$. The left is at Mn=0.08, the right at Mn=0.002, and the views are along the field direction (z axis).

3. A comparison shows that Eq. 22 is a good approximation to the exact the radial and tangential fragmentation energies.

4. Solutions to the self consistent Eq. 33 (curves) are compared to Eq. 28. In each case the feature of low chain angle, and thus stress, at small Mn is observed, but the self-consistent solutions soften the effect.

5. Uniaxial simulation data make a master curve on axes suggested by Eq. 28. The data at $\lambda=3.3$ (to the left) do not collapse as well as the others ($\lambda=6.3$, 8.8, 10.7, 16.7, 29.6), but this is expected based on Eq. 33.
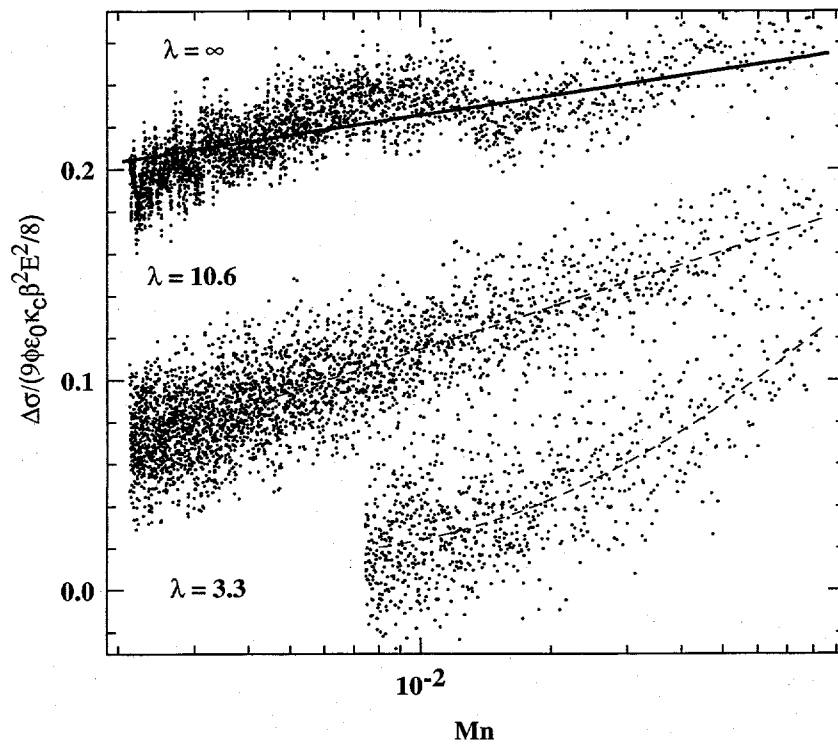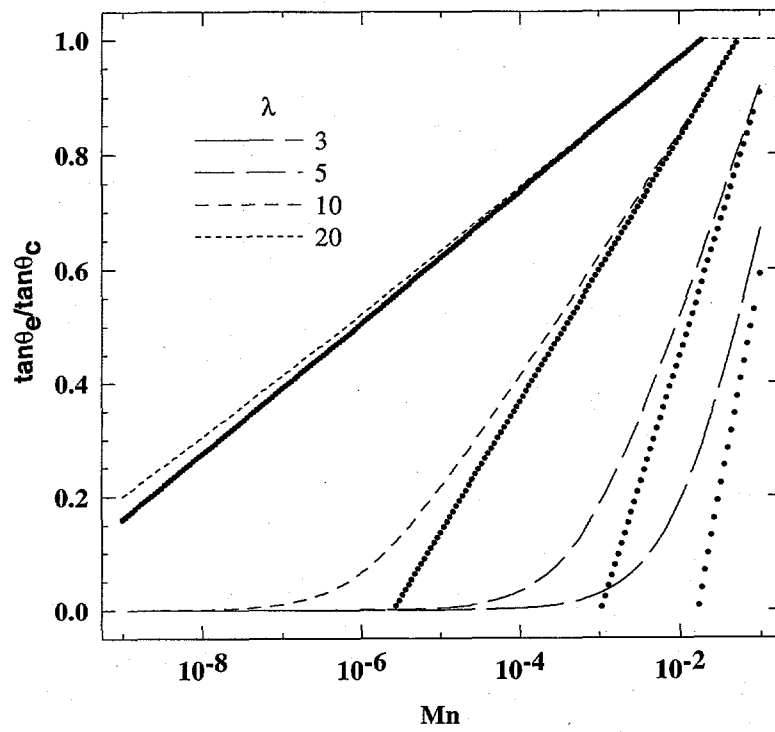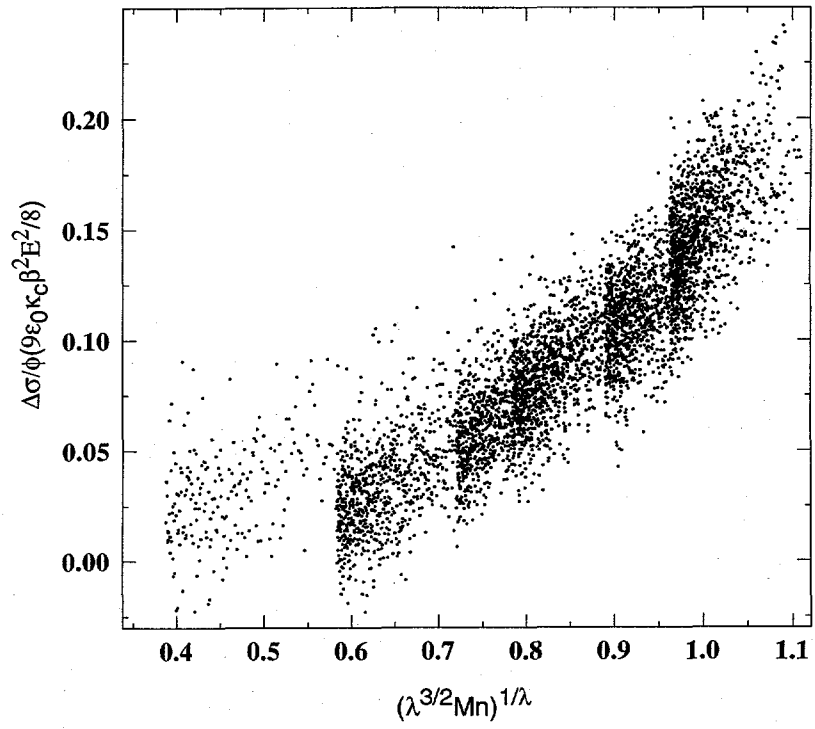
Martin - Fig. 1
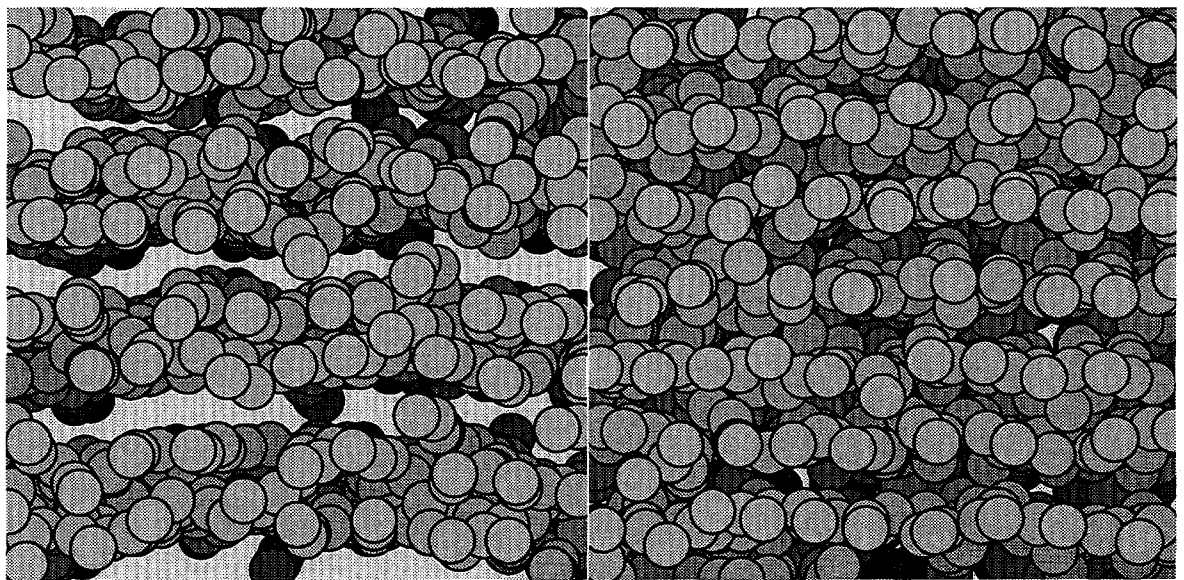
Martin – Fig. 2
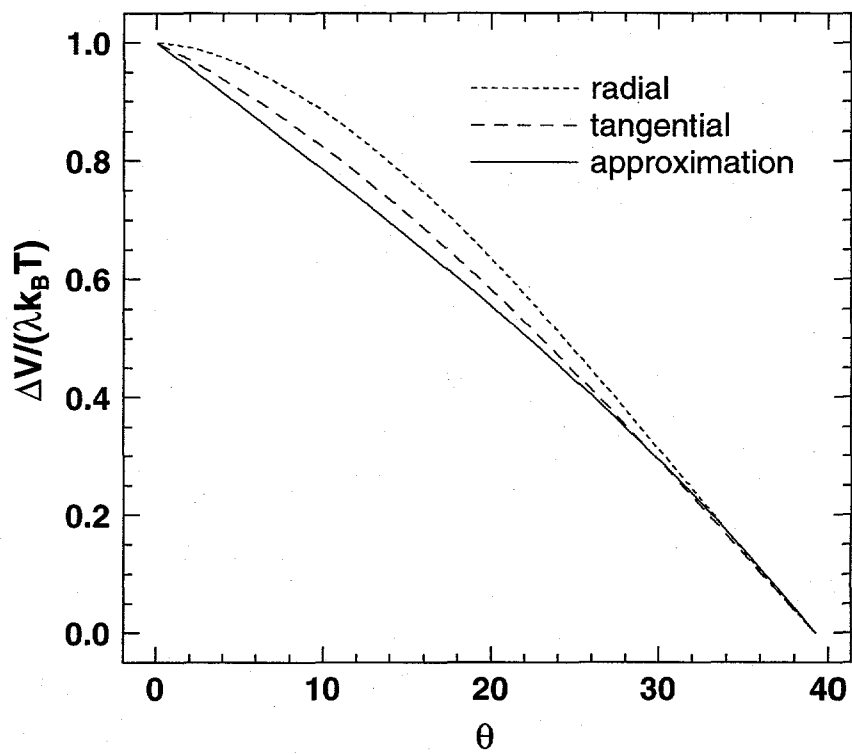
Martin - Fig. 3

Martin – Fig. 4

Martin – Fig. 5